DOI: 10.1002/ ((please add manuscript number))
Article type: Full Paper

Wetting state transitions over hierarchical conical microstructures

*Il Woong Park, Maria Fernandino, and Carlos A. Dorao**

Høgskoleringen 1, 7491, Trondheim, Norway
E-mail: carlos.dorao@ntnu.no

Keywords: hierarchical cone, microstructure, wetting transition

Advancing in a better understanding of physics of wetting requires to be able to develop surfaces with well-controlled roughness by controlling the microstructure morphology. In this study, patterned truncated cones and hierarchical conical structures were fabricated. The wetting properties of the fabricated surfaces were measured for identifying the importance of the geometrical parameters on the wetting states ranging from superhydrophobic to superhydrophilic. In particular, the wetting transition from Cassie-Baxter to Wenzel state and its dependence on the geometrical parameters was investigated. It was observed that the transition is dependent on the center-to-center distance and the height of the structures.

1. Introduction

The wettability of a surface is a fundamental physical property with relevance in many scientific and industrial applications [1-2]. It has been observed that many surfaces in nature exhibit superhydrophobic and superhydrophilic characteristics tailored to some particular functionality [3-4]. The properties of such surfaces have motivated researchers mimicking them with the goal of developing novel surfaces with customized properties [5-7]. However, major challenges have remained related to the fabrication techniques for achieving optimal controllability of the properties of the surfaces which can also contribute to a better understanding of the wetting phenomena [5].

Recent progress in fabrication techniques has been allowing a precise control of the surface properties in particular in terms of shape and size for studying wetting phenomena [8-15]. For example, Liu and Kim [8] fabricated a superhydrophobic surface with a doubly re-entrant nano overhangs structure. This surface has shown a high apparent contact angle even for liquids with low surface tension. Chu et al. [9] fabricated surfaces with micropillars and hierarchical structures showing a superhydrophobic state. In addition, a negative relation between the apparent contact angle and the dynamic contact angle was observed. Xue et al. [14] fabricated microcones by the inclined etching method for studying the effect of geometrical parameters of microcones on the apparent contact angle, contact angle hysteresis and sliding angle. Cai et al. [15] studied the effect of the geometrical parameters of the microstructures and side wall angle on the wetting properties. In particular, it was observed that the microstructures having a side wall angle lower than 90 degrees give higher contact angle compared with the microstructures having side wall angle higher than 90 degrees.

The wetting phenomena in roughened surfaces are normally referred to the Wenzel and Cassie-Baxter models [16-19]. The Wenzel state describes a homogeneous wetting regime where the liquid is contacting with the surface, while the Cassie-Baxter state describes a regime where empty volume between a liquid droplet and solid surface is observed. Several research studies have focused on understanding the transition between the Cassie-Baxter state and the Wenzel state (Cassie-Wenzel transition) [20-26]. Especially, there was an effort to understand to maintain the Cassie wetting state stable [27]. However, there is no common agreement about the underlying physical phenomena controlling each state and its transition. The transition has been explained in terms of the threshold of the energy barrier, meniscus touching on the substrate, air cushions beneath the droplet and critical pressure.

The control of the Cassie-Wenzel transition between superhydrophilic and superhydrophobic surfaces can contribute to the design surfaces with customized properties in a diverse range of applications. At the same time, controlling the Cassie-Wenzel transition can help to improve

the understanding of the wetting states transition. For this reason, experimental studies have tried to control the Cassie-Wenzel wetting transition by an external excitation such as vibration or electricity [28-30]. However, such active approaches for controlling the Cassie-Wenzel wetting can present limitations in some applications. This fact has motivated the need for controlling the Cassie-Wenzel wetting in a passive manner by varying the geometrical parameters of the surface without external excitations. The stable condition of the Cassie-Wenzel state could be helpful for the potential application on microfluidics [31].

The aim of this study is to fabricate surfaces presenting superhydrophobic and superhydrophilic states with a broad range of geometric parameters. The selected surfaces are motivated in conical structures observed in nature [4] showing both superhydrophilic and superhydrophobic properties. And also a fabrication of the structure with the silicon substrate in conical shape could be beneficial in terms of the mechanical response [32]. Two type of structures are considered in this study namely truncated cones and hierarchical conical structures as structures with lower than 90 degrees of sidewall angle have an advantage on achieving high apparent contact angle [15]. In order to cover both superhydrophobic and superhydrophilic states the height and center-to-center distance of the structures were controlled. The fabrication of the samples is based on photolithography and cryogenic Reactive Ion Etching (RIE). The wetting properties and wetting transition of the fabricated surfaces are measured and correlated with the geometrical properties.

2. Results and Discussion

Both truncated cone and hierarchical cone were fabricated by lithography and dry etching process as shown in **Figure 1**. Each surface with micro cone has 3 types of height which are 35, 55, 75 µm and 16 types of center-to-center distance between cone from 15 µm to 360 µm. The apparent contact angle and the contact angle hysteresis were measured. **Figure 2a** shows the apparent contact angle and the contact angle hysteresis with a varying center-to-center

distance of the truncated cones and hierarchical cones with a height of 75 µm, named TC75 and HC75 samples respectively. The terminology of the apparent contact angle was defined and clarified by Marmur et al [33]. From this approach, it was able to avoid a misunderstanding by measuring the apparent contact angle with the hypothetical heterogeneous surface. The x-axis represents the center-to-center distance of truncated cones and the y-axis represents the apparent contact angle and contact angle hysteresis. The apparent contact angle of truncated cone is represented by open black squares while hierarchical cones are represented by up-pointing triangles. The center-to-center distance is varied from 15 µm to 360 µm observing three distinctive regions for of truncated cone, i.e. TC75 samples. The first region corresponds to the Cassie-Baxter state for the center-to-center distance from 15 µm to 60 µm. The apparent contact angle and contact angle hysteresis of the Cassie-Baxter state shows a linear dependency of the center-to-center distance. The second region corresponds to the Cassie-Wenzel transition corresponding to center-to-center distance from 60 µm to 70 µm. The apparent contact angle decreases abruptly in this region. This trend has also been observed for flat-top micro pillars [24]. Finally, the third region corresponds to the Wenzel state and the contact angle shows independence of the center-to-center distance of the cones.

The hierarchical cones, i.e. HC75 samples, shows three distinctive regions. The first region corresponds to the Cassie-Baxter state for the center-to-center distance from 15 µm to 50 µm, i.e. coinciding with the truncated cones. The apparent contact angle of the truncated cones and hierarchical cones are similar in the Cassie-Baxter state indicating that the microstructure has no influence in the contact angle. The area fraction or the roughness of the contacting surface on the top part can be considered an important parameter controlling the apparent contact angle in Cassie-Baxter state. The second region corresponds to a sharp Cassie-Wenzel transition occurring for the center-to-center distance from 50 µm to 60 µm, i.e. quite similar to the case of truncated cones. The third region corresponds to a superhydrophilic state. It is remarkable that the surface with hierarchical cones shows a transition from the

superhydrophobic state to the superhydrohpilic state by a change in the center-to-center distance. In particular, the transition occurs in less than 10 μm of the center-to-center distance. Results for the contact angle hysteresis for truncated cone and hierarchical cone are depicted as the red diamond with a dot in the center and down-pointing triangle with a dot in the center in Figure 2a. Both truncated cone and hierarchical cone shows decreasing and overlapping contact angle hysteresis with increasing center-to-center distance in the Cassie-Baxter state. Similar to the apparent contact angle, the hierarchical structure has no apparent influence on the contact angle hysteresis. In terms of applicability, a low contact angle hysteresis surface possesses the property of self-cleaning when the apparent contact angle is high. In this sense, the fabricated surface shows a decreasing contact angle hysteresis and increasing apparent contact angle between 15-60 μm of center-to-center distance. Therefore, a surface with low contact angle hysteresis and high apparent contact angle for self-cleaning applications can be fabricated by modifying the spacing of microstructures. At the Cassie-Wenzel transition, the contact angle hysteresis shows a sharp increase, and then the contact angle hysteresis decreases for the case of the truncated cones while slightly increases for the case of the hierarchical cones. In the Figure 2a, it is possible to see that the advancing angle and receding angle were measured as zero for the cases of 60 and 70 μm of center-to-center distance because a droplet was soaked fast into the surface. These two samples show zero apparent contact angle with zero contact angle hysteresis.

Figure 2b shows both apparent contact angle and contact angle hysteresis of truncated cones and hierarchical cones with a height of 55 μm, named TC55 and HC55 samples respectively. In general, similar characteristic compared to the TC75 and HC75 samples are observed. However, for the case of the hierarchical cones with 50 and 60 μm of center-to-center distance impregnating Cassie state [16] are observed. It seems like that there was a lack of the volume between the structures to be a superhydrohpilic state, and the leftover liquid which wasn't soaked between structures formed a droplet on top of the impregnating surface.

In **Figure 2c**, the apparent contact angle and the contact angle hysteresis of truncated cones and hierarchical cones with a height of 35 µm, named TC35 and HC35 samples respectively. In this samples, the hydrophobic state was not observed. It could be assumed that there is threshold height of the microstructure or volume of the air cushion for maintaining droplet in Cassie-Baxter state. In these samples, impregnating Cassie state were observed in both truncated and hierarchical cone.

In **Figure 2d** the apparent contact angle and the contact angle hysteresis for the Cassie-Baxter state are highlighted. The apparent contact angle and contact angle hysteresis show an opposite trend on the center-to-center distance as observed by Chu [9] and Xue [14]. The highest apparent contact angle of 167 degrees with a contact angle hysteresis of 16 degrees of was achieved with the truncated cone with 60 µm of center-to-center distance. In terms of the lotus effect, a higher apparent contact angle and lower apparent contact angle are desired. The plot shows that the apparent contact angle and contact angle hysteresis are in negative relation. There is a difference of 10 µm of center-to-center distance between the truncated cone and hierarchical cone in terms of the location of the Cassie-Wenzel transition. And there were differences of 10 µm of center-to-center distance between 75 µm of the height of the micro conical structures and 55 µm of them. In summary, this plot shows that the surface with truncated cones with higher structures provides the Cassie-Baxter state in higher center-to-center distance condition. For achieving the desired wetting state with respect to the lotus effect, it seems like that higher center-to-center distance provides higher apparent contact angle with lower contact angle hysteresis. Thus, fabrication of high truncated cones could be a solution for fabricating a surface with a high apparent contact angle with low contact angle hysteresis.

Figure 3a and 3b illustrate different wetting states for the truncated cone and for the hierarchical cone in this study. In the figure, the x-axis represents the center-to-center distance between truncated cones and the y-axis represents the height of the truncated cone. Four

different wetting states which are the Cassie-Baxter state, the Wenzel state, Superhydrophilic state, and the impregnating Cassie state represent the following geometric condition of the microstructure. As reported by Liu [25] and Shahraz [26], the apparent contact angle or the wetting states could be connected with structural or morphological parameters such as a height, a ratio between diameter, pitch and groove width. Both theoretical studies show that the Cassie-Baxter state exists where the spacing between the structures is low which is also observed in this work. In terms of the height of the microstructure, it was reported that the Cassie-Baxter state is observed when the height of the structure is high according to Shahraz [26]. The Cassie-Wenzel transition is not affected by the height of the structures as reported by Liu [25].

The map depicts that the Cassie-Wenzel transition could occur due to changes in both height and spacing of the structures. Barbieri [24] has observed that the transition from the Cassie-Baxter state to Wenzel state can be occurred by increasing the pitch and decreasing the height of the structure. The map also shows the occurrence of superhydrophilic and impregnating Cassie state. It was possible to observe that an existence of the hierarchical structures transforms the Wenzel state to superhydrophilic or the impregnating Cassie state by comparing two graphs. Furthermore, it shows that the existence of the hierarchical structures enhances the spreading of the liquid. It was observed that there is the change between the superhydrophilic and impregnating Cassie state in the sample with hierarchical cones. It could be hypothetically explained that the change between two states could be decided by the amount of the volume between the microstructures which can capture the liquid. This could be the reason why the superhydrohpilic state was able to be achieved when the condition is in the upper right corner which is representing the large volume between the structures in the graph. It could be concluded that the geometric parameter has a significant effect on the wetting states and the wetting transition.

Furthermore, experimental results can be presented based on the developed model for wetting transition from the previous study. A variation of the depinning pressure was obtained numerically and it was validated with the theoretical results by Blow and Yeomans [34]. It has been observed that the high spacing between the structures can cause the low-pressure drop for leading to collapse the droplet. Based on this model, the critical pressure was calculated to present experimental result in this study as shown in Figure 4. The used model for the critical pressure can be written in equation (1), where the D_T is the diameter of the top surface of the microstructure, γ is the surface tension, θ_A is the apparent contact angle and the P is the spacing between the micro structures.

$$\Delta P_{critical} = \frac{-2\pi D_T \gamma cos\theta_A}{P^2 - \pi {D_T}^2} \quad (1)$$

In this calculation, geometric parameters from the experiment were adopted and the measured apparent contact angle in case of TC55 was applied. It shows that increasing spacing could cause the low critical pressure and also the low critical pressure could collapse the hydrophobic state.

Two types of the breakdown of Cassie-Baxter state which were observed in this experiment could be compared with the developed models in previous studies. Two types of the breakdown which are due to the increased spacing between the microstructures and the decreased height of the microstructure could be identified. The first type of the breakdown could be explained with the concept of the critical pressure [34, 35]. As presented in **Figure 4**, the critical pressure for leading the collapse becomes low when the spacing between the structures become high.

To identify the effect of the height regarding on the breakdown of the hydrophobicity, the model with the height of microstructure should be considered. In the concept of the sag transition [36, 37], there is a model for the minimum height to avoid the sag transition and to maintain the Cassie state was suggested by Patankar et al [36]. The sag transition can occur

when the bent liquid-gas interface touches the solid surface. It could occur when the height of the structure is not high enough in order to avoid the touch-down between the liquid-gas interface and the solid surface. In the sag transition, it was assumed that the bending of the liquid-gas interface oriented from the corner of the microstructures. The minimum height to avoid the sag transition was calculated based on the geometrical parameter from the experiment as shown in **Figure 5**. The used model for the critical pressure can be written in equation (2) and (3).

$$H = R\left(1 - \sqrt{1 - \frac{P^2}{2R^2}}\right) \quad (2)$$

$$R = \frac{2P(1 + \frac{P}{2D_T})}{-2cos\theta_A} \quad (3)$$

In this calculation, the apparent contact angle was assumed as 150 degrees. If the sag distance was calculated in a range between 35 µm and 55 µm, it could be concluded that the sag transition was the dominant effect to breaks the hydrophobicity in this experiment. However, the calculated sag distance based on the model was less than 6 micrometer. It could imply that the sag transition was not the dominant effect to collapse the hydrophobicity in this experiment and the other mechanism such as a depinning transition could be the reason for the breakdown of the hydrophobicity when the height of the structure decreased.

4. Conclusion

Micro conical structures with well-organized geometric parameters have been fabricated by photolithography and RIE process. In total 96 different samples were fabricated comprising two structure types, three heights, and sixteen center-to-center distance. Different wetting properties were identified ranging from superhydrophobic state to superhydrophilic. In the case of superhydrophobic state surfaces with high apparent contact angle and low contact angle hysteresis were obtained. With regard to the lotus effect, it has been observed that a

path for fabricating a surface with a high apparent contact angle with low contact angle hysteresis can be achieved with high truncated cones. Furthermore, a drastic wetting transition from Cassie-Baxter state to Wenzel state was observed in the case of hierarchical cones compared to the more gradual transition for the case of truncated cones. It is important to note that the transition was not forced by external excitation but instead due to changes in the geometrical characteristics of the surface. Finally, the present study cover geometrical structures over a scale of the dozens of micrometers compared to previous studies limited to a more narrow range of dimensions opening the possibility of bringing a broader view of the surface wettability problem.

For the further study, it could be more challenging to overcome the oleo-repellency compared with the water-repellency. This is because of the surface tension of the oil usually lower than that of the water. It has been observed that the superoleophobic surface can be obtained with the hierarchical nano-scaled topography of fluorinated polyethylene surface by the plasma etching [38]. An identification of the oleophobicity by changing the geometric parameter of the hard microstructures could be meaningful in order to explore the wetting transition.

4. Experimental Section

4. 1. Fabrication procedure of micro conical structures

The challenge in the present work was to fabricate two types of conical structures namely truncated cones and hierarchical cones. The main challenge in this work is to have control of the position of the relatively large micro conical structures called truncated cones and being able to add small micro conical structures on top of the previous one for producing the hierarchical cones.

The structures were fabricated on top of a silicon wafer using photolithography and dry etching. Single-side polished silicon wafers ({100}, P-type, containing boron as dopant) were prepared for constructing microstructures. The silicon wafer was rinsed with ethanol, isopropanol (IPA), acetone, deionized water in sequence and then dried with the N2 flow. Additionally, the wafer was treated with oxygen plasma for 3 minutes in order to remove impurities and contaminants in a plasma chamber (Diener Electronics Femto). After the cleaning steps, photolithography was conducted for imprinting patterns on top of the wafer. For this process a film of 4 μm thickness of SU-8 negative photoresist from MicroChem was spin-coated. After spin-coating, the wafer was baked on the heating plate for 1 minute at 65°C and 2 minutes at 95°C. After the pre-baking step, Ultraviolet (UV) light exposure was conducted on top of the coated wafer. In this exposure step, a photomask which is a 5-inch chrome glass mask (Micro Lithography Services, UK) was placed between the UV light source and the silicon wafer. There were sixteen patterns of circles in the square grid on top of the photomask. These patterns were imprinted on top of the wafer by exposing UV light with a Mask Aligner (Karl Süss, MA-6). A wavelength of 365 nm and 200 mJ/cm2 of exposure dose were used as parameters for the UV exposure. After UV light exposure, the wafer was baked again on the heating plate for 1 minute at 65°C and 2 minutes in 95°C. The patterns on the wafer were developed in Mr-DeV 600 (Micro Resist Technology GmbH, Germany) bath. After the development step, the wafer was cleaned with IPA and deionized water in sequence and dried with the N2 flow. By following this procedure pillars of SU-8 in size of 9 μm of diameter and 4 μm of height were constructed on top of the silicon wafer as shown in Figure 1a. The conical structures were fabricated based on these SU-8 pillars.

The hierarchical conical structures were fabricated by two steps of cryogenic Reactive Ion Etching (RIE) processes. The first RIE process step produced the large truncated cones and the second RIE process step added the micro cones to the surface. The two RIE steps were done in an ICP-RIE Cryo Reactor (Plasmalab 100 - ICP180, Oxford Instruments, U.K.). The

fabrication of the cones is achieved by controlling the etching profile such that the side wall angle is less than 90 degrees. This side wall angle and the taper angle are highly dependent on cryogenic temperature and composition of gas flows [39, 40]. In particular, micro cones can be generated with a random distribution with the RIE process [41]. In the present work, the etching recipe was developed for fabricating only large truncated cones at precise locations determined by the SU-8 pillars suppressing the random generation of micro cones. The etching parameters were developed for achieving the desired side angle of etching profile while suppressing of randomly generated structures. Etching parameters including Capacitive Coupled Plasma (CCP) Radio Frequency (RF) power, Inductively Coupled Plasma (ICP) power are described as first RIE in **Table 1**. For producing small cones, black silicon method was selected [42]. It was reported that DRIE etching process is suitable for producing small-size structures on top of the microstructures [43, 44]. Selected parameters for second RIE process are described in Table 1.

In summary, truncated cones TC were obtained after a first RIE step with three different heights of 35, 55 and 75 μm on top of the silicon wafer and the samples are named TC35, TC55, and TC75 respectively. Each TC35, TC55, and TC75 set include sixteen samples with different center-to-center distances. A SEM image of TC55 is shown in **Figure 1b**. In the figure, it is able to observe truncated cones on top of the silicon surface and SU-8 pillars on top of the truncated cones. The hierarchical conical structures were obtained by adding a second RIE process to TC35, TC55, and TC75 samples. The samples are named HC35, HC55, and HC75 following the height of the truncated cones. SEM images of HC55 and HC75 are shown in Figure 1c and 1d. Small structures were produced not only on the bottom surface between truncated cones but also on the side surface of truncated cones. In this process, the bottom and the side surfaces were roughened selectively when the top surface of SU-8 was kept as a smooth surface. Parameters of the microstructures are described in **Table 2**. The main parameters of the structures are height of the truncated cone HT, height of photoresist

HP, height of silicon HC, diameter of top surface of truncated cone DT, diameter of bottom part of conical structure DB, and center-to-center distance P. In total, 96 samples (48 samples of truncated cone and 48 samples of hierarchical cone) were prepared for identifying wetting parameters.

We used the silicon substrate of the silicon wafer {100} as hard microstructures. Silicon-based microfabrication could be important to overcome the robustness of the microstructures. The hard matter as a rigid solid part could give more consistent interaction between the liquid in terms of the three-phase contact line compared with the soft matter which could be deformed as an elastic solid substrate. It could be the reason why we observed the drastic wetting transition with changing the geometric parameter with the hard solid substrate.

It could be helpful to discuss the reproducibility and the shelf-life of the samples. In case of the lithography step, it was able to obtain close geometrical parameters of the photoresist structures. However, reproducing of the conical shape in dry etching step should be considered much sensitively. It means that the same etching recipe could not provide identical geometrical parameters of the cones. This is because the condition of the chamber of the cryo affects the etching profile sensitively. For easier reproduction, it was important to make the chamber condition stable, by repeating cleaning steps and etching steps with a bare wafer. After this, the amounts of the oxygen and sulfur hexafluoride which are dominant parameters for deciding the sidewall angle could be adjusted for obtaining targeted sidewall angle of the structures by trial and error. In order to check the shelf-life of the structures, SEM images of the samples were obtained again after 10 months. In the SEM images, there was no significant change after 10 months.

4. 2. Scanning Electron Microscopes (SEM)

An FEI Helios dual-beam Focused Ion Beam Scanning Electron Microscopes (FIB-SEM) was used to characterize microstructures. Especially, the height of microstructures was measured by tilting the sample 52 degrees inside the microscope. 15 kV and 20 kV of voltages were used for taking SEM images. This is because there was a deformed image of the SU-8 part due to the scattering in low voltage condition such as 5 kV or 10 kV.

4. 3. Contact angle measurement

The apparent contact angle and the dynamic contact angle was measured for each sample. An optical tensiometer (Attension Theta, Biolin Scientific, Sweden) was used for measuring contact angles. The apparent contact angle was measured with 12.6 μL of gently dropped distilled water droplet. Droplets were generated with a rotating type of syringe (Hamilton Co, Reno Nevada, U.S.). For obtaining contact angle hysteresis, an advancing and receding angles were measured with a changing volume of the DI water. Both sessile and meniscus options were applied depending on the shape of liquid on the surface. After measuring the apparent contact angle of the droplet, the contact angle hysteresis was obtained by measuring advancing and receding contact angle. For measuring two contact angles the needle penetrated softly into the droplet. After inserting the needle, the liquid was injected and ejected for changing the volume of the liquid. The liquid was injected from 10 to 80 μl for measuring the advancing angle and ejected from 40 to 5 μl for measuring the receding angle. By recording the high-speed images, the advancing and receding angle of the droplet was obtained when the volume of the liquid was changing. For the contact angle hysteresis, the reproducibility was focused during the experiments. From this, the minimum and maximum point were obtained when the minimum or maximum dynamic contact angle can be obtained in repeat test.

4. 4. Apparent contact angle of reference surfaces

As the fabricated surfaces are presenting particular properties, the local wetting properties of each surface type which are the top surface of truncated cone, the bottom surfaces between truncated cones with and without the small cones are evaluated as a reference surface. For this evaluation, three different surfaces were treated by the same RIE processes but without the patterned SU-8 pillars resulting in reference surfaces mimicking the local characteristics of the conical surfaces. For fabricating the first reference surface, the silicon surface was treated by 20 and 40 minutes of the first RIE process. After this etching, the apparent contact angles were measured as 54 and 58 degrees. This wetting property represents the bottom surface between truncated cones when the small cones are not present. For the second reference surface, the second RIE process was conducted on the previous reference surfaces. The apparent contact angles of the second reference surfaces were measured as 62 and 65 degrees. The apparent contact angles of the second reference surfaces are in good agreement with a previous study [45] which shows an apparent contact angle of 62.3 degrees for a black silicon surface. The second reference surface represents the bottom surface between truncated cones when the small cones are present. For the third reference surface, a wafer was spin-coated with a uniform layer of SU-8 that was baked and exposure by UV light without a mask. After this step, the surface was treated by both types of RIE processes showing an apparent contact angle 66 degrees. The apparent contact angle was measured to be less than 2 degrees before and after the etching process. This wetting property represents the top surface of the SU-8 surface on top of the truncated cones. During the fabrication steps, the small differences in the apparent contact angle between the reference surfaces were considered. The parameters for both RIE steps were adjusted based on the wetting properties of the reference surfaces. As a consequence, the three reference surfaces have an apparent angle in the range from 54 to 66. From this, it was possible to avoid significant differences of wetting properties between the local surfaces of micro conical structures. This is because the polished silicon surface which is expected to exist on a top surface of a structure where the SU8 is removed has a hydrophilic

state. In short, the SU8 has a role in controlling the local wetting condition in the similar range.

Acknowledgements

The Ph.D. fellowship (Il-Woong Park) financed by the NTNU-SINTEF Gas Technology Centre is gratefully acknowledged. The Research Council of Norway is acknowledged for the support to the Norwegian Micro- and Nano-Fabrication Facility, NorFab, for the fabrication and characterization of samples at the NTNU Nanolab facility.

Received: ((will be filled in by the editorial staff))

Revised: ((will be filled in by the editorial staff))

Published online: ((will be filled in by the editorial staff))

References

[1] Z. Wang, M. Elimelech, S. Lin, *Environ. Sci. Technol*. **2016**, *50*, 5.

[2] L. Wen, Y. Tian, L. Jiang, *Angew. Chem. Int. Ed.* **2015**, *54*, 11.

[3] W, Barthlott, C. Neinhuis, *Planta* **1997**, *202*, 1.

[4] K. Koch, W. Barthlott, *Philos. Trans. R. Soc., A.* **2009**, *367*, 1893.

[5] Y. Y. Yan, N. Gao, W. Barthlott, *Adv. Colloid Interface Sci.* **2011**, *169*, 2.

[6] L. Zhang, N. Zhao, J. Xu, *J. Adhes. Sci. Technol.* **2014**, *28*, 8.

[7] C. Frankiewicz, D. Attinger, *Nanoscale* **2016**, *8*, 7.

[8] T. Liu, C. J. Kim, *Science* **2014**, *346*.

[9] D. Chu, A. Nemoto, *Appl. Surf. Sci*. **2014**, *300*, 117.

[10] H. Bellanger, T. Darmanin, E. Taffin de Givenchy, F. Guittard. *Chem. Rev. (Washington, DC, U. S.)* **2014**, *114*, 5.

[11] H. Ems, S. Ndao, *Appl. Surf. Sci.* **2015**, *339*, 137.

[12] M. Kanungo, S. Mettu, K.Y. Law, S. Daniel, *Langmuir* **2014**, *30*, 25.

[13] S. Utech, K. Bley, J. Aizenberg, N. Vogel, *J. Mater. Chem. A.* **2016**, *4*, 18.

[14] P. Xue, J. Nan, T. Wang, S. Wang, S. Ye, J. Zhang, Z. Cui, B. Yang, *Small* **2016**, *13*, 4.

[15] T. M. Cai, Z. H. Jia, H. N. Yang, G. Wang, *Colloid Polym. Sci.* **2016**, *294*, 5.

[16] E. Bormashenko, *Adv. Colloid Interface Sci.*, **2015**, *222*, 92.

[17] B. N. Young, *Colloids Surf. A* **2009**, *345*, 1.

[18] R.N. Wenzel, *Ind. Eng. Chem.* **1936**, *28.8*, 988.

[19] A.B.D. Cassie, S. Baxter, *Trans. Faraday Soc.* **1944**, *40*.

[20] D. Murakami, H. Jinnai, A. Takahara, *Langmuir* **2014**, *30*, 8.

[21] P. Papadopoulos, L. Mammen, X. Deng, D. Vollmer, H. J. Butt, *Proc. Natl. Acad. Sci. U. S. A.* **2013**, *110*, 9.

[22] T. Koishi, K. Yasuoka, K. S. Fujikawa, T. Ebisuzaki, X. C. Zeng, *Natl. Acad. Sci. U. S. A.* **2009**, *106*, 21.

[23] Q. S. Zheng, Y. Yu, Z. H. Zhao, *Langmuir* **2005**, *21*, 26.

[24] L. Barbieri, E. Wagner, P. Hoffmann, *Langmuir* **2007**, *23*, 4.

[25] T. Liu, Y. Li, X. Li, W. Sun, *J. Phys. Chem. C* **2017**, *121*, 18.

[26] A. Shahraz, A. Borhan, K. A. Fichthorn, *Langmuir* **2012**, *28*, 40.

[27] G. Whyman, E. Bormashenko, *Langmuir* **2011**, *27*, 8171

[28] W. Lei, Z. H. Jia, J. C. He, T. M. Cai, *Appl. Phys. Lett.* **2014**, *104.18*, 181601.

[29] G. Liu, L. Fu, A.V. Rode, V.S. Craig. *Langmuir* **2011**, *27*, 6.

[30] N. Kumari, S. V. Garimella, *Langmuir* **2011**, *27*, 17.

[31] Z. Liu, Y. Wu, B. Harteneck, D. Olynick, *Nanotechnology* **2012**, *24*, 1.

[32] K. Sekeroglu, U. A. Gurkan, U. Demirci, M. C. Demirel, *Appl. Phys. Lett.* **2011**, *99*, 063703.

[33] A. Marmur, C. Della Volpe, S. Siboni, A. Amirfazli, J. W. Drelich, *Surf. Innov*. **2017**, *5*, 3.

[34] M. L. Blow, J, M, Yeomans, *Int. J. Mod. Phys. C* **2012**, *23*, 1240013.

[35] M. J. Hancock, M. C. Demirel, *MRS Bull.* **2013**, *38*, 391.

[36] N. A. Patankar, *Langmuir* **2010**, *26*, 8941.

[37] B. Liu, F. F. Lange, *J. Colloid. Interface. Sci*. **2006**, *298*, 899.

[38] E. Bormashenko, R. Grynyov, G. Chaniel, H. Taitelbaum, Y. Bormashenko, *Appl. Surf. Sci*. **2013**, *270*, 98.

[39] E. So, M. C. Demirel, K. J. Whal, *J. Phys. D. Appl. Phys*. **2010**, *43*, 045403.

[40] F. Saffih, C. Con, A. Alshammari, M. Yavuz, B. Cui, *J. Vac. Sci. Technol., B: Nanotechnol. Microelectron.: Mater., Process., Meas., Phenom*. **2014**, *32*, 6.

[41] V. Kondrashov, J. Rühe, *Langmuir* **2014**, *30.15*, 4342.

[42] H. Jansen, M. de Boer, R. Legtenberg, M. Elwenspoek, *J. Micromech. Microeng*. **1995**, *5.2*, 115.

[43] K. Rykaczewski, A. T. Paxson, S. Anand, X. Chen, Z. Wang, K. K. Varanasi, *Langmuir* **2013**, *29*, 3.

[44] G. Sun, T. Gao, X. Zhao, H. Zhang, *J. Micromech. Microeng.* **2010**, *20*, 7.

[45] L. X. Yang, Y. M. Chao, L. Jia, C. B. Li, *Appl. Therm. Eng.* **2016**, *99*, 253.

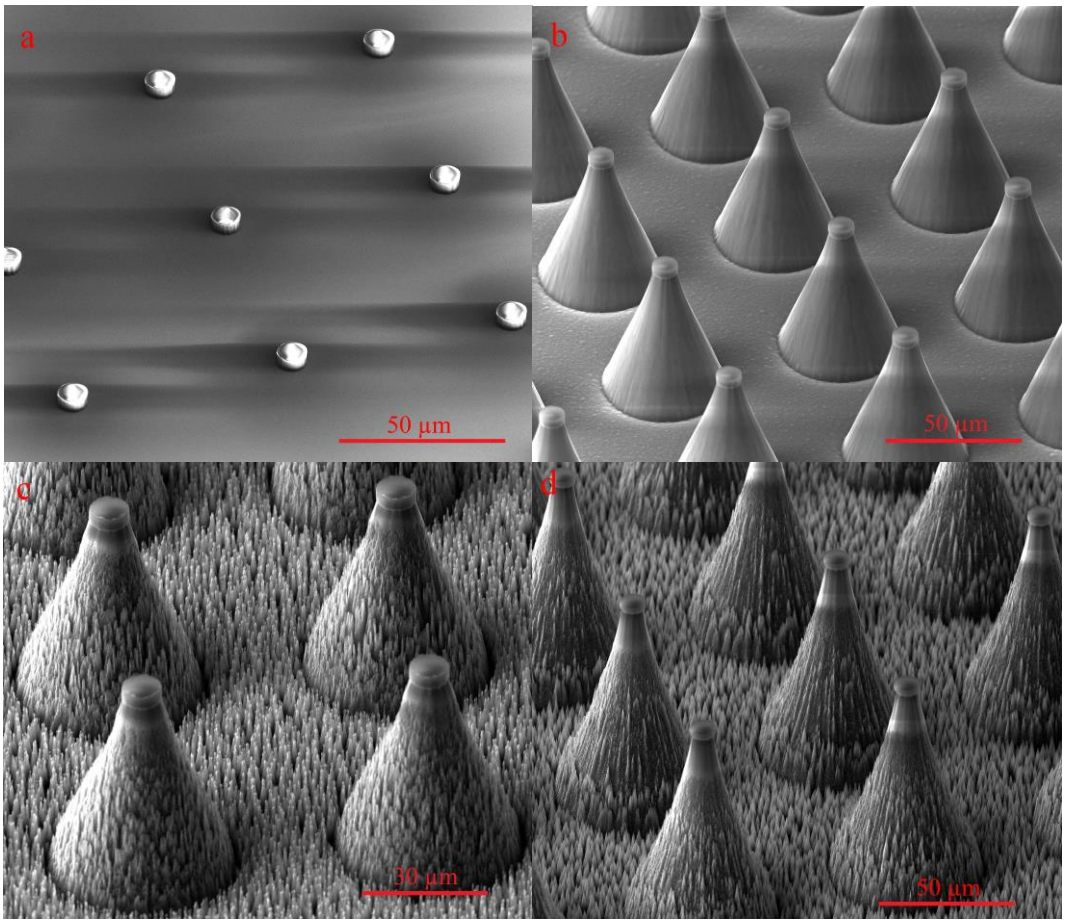

Figure 1. SEM images of micro conical structures. (a) SU-8 structures (4 µm of height). (b) Truncated micro cones (55 µm of height). (c) Hierarchical micro conical structures (55 µm of height). (d) Hierarchical micro conical structures (75 µm of height).

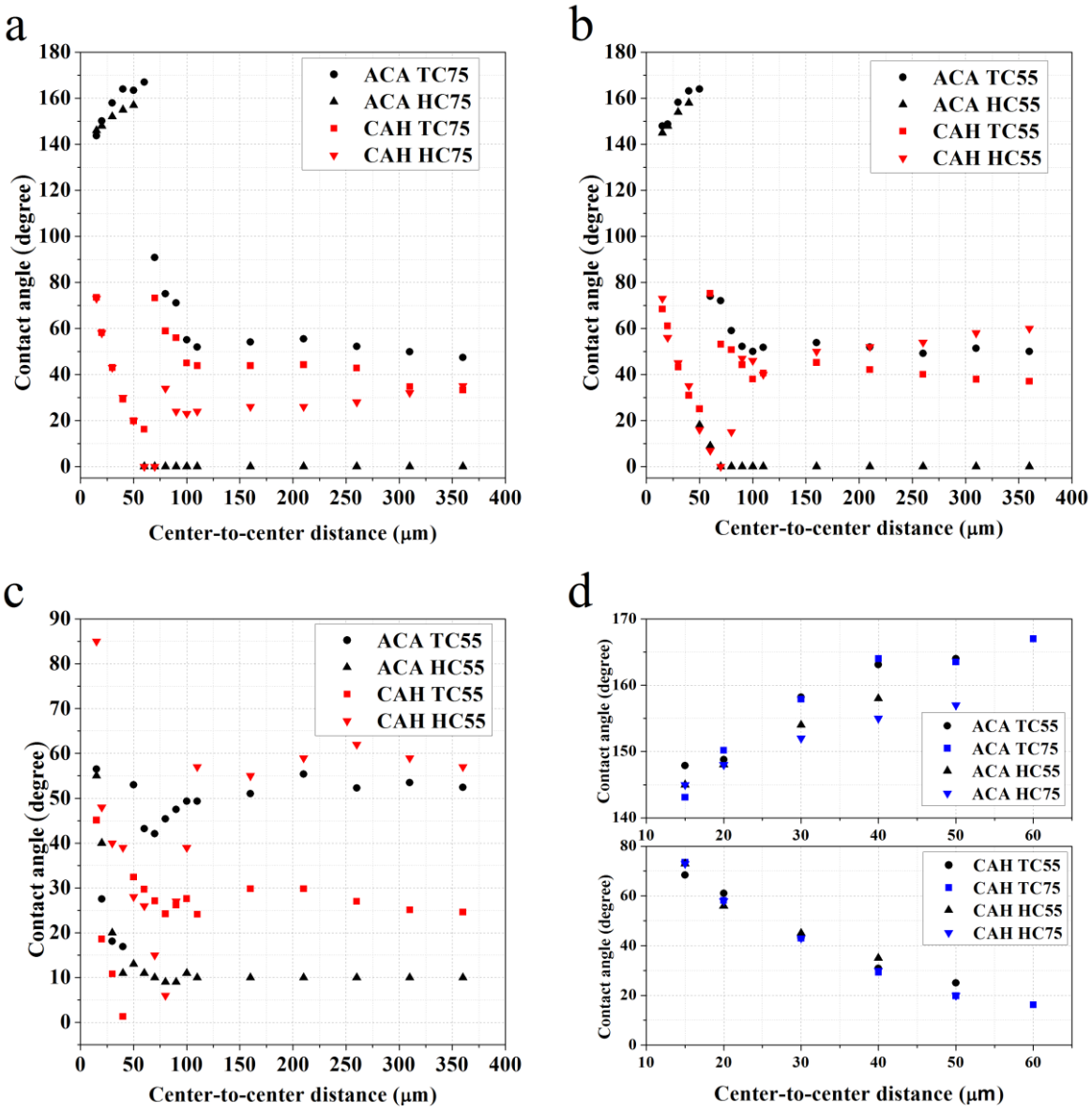

Figure 2. Apparent Contact Angle (ACA) and Contact Angle Hysteresis (CAH) of Truncated Cone (TC) and Hierarchical cone (HC) of (a) 75 μm of height, (b) 55 μm of height, (c) 35 μm of height, and (d) Cassie-Baxter state.

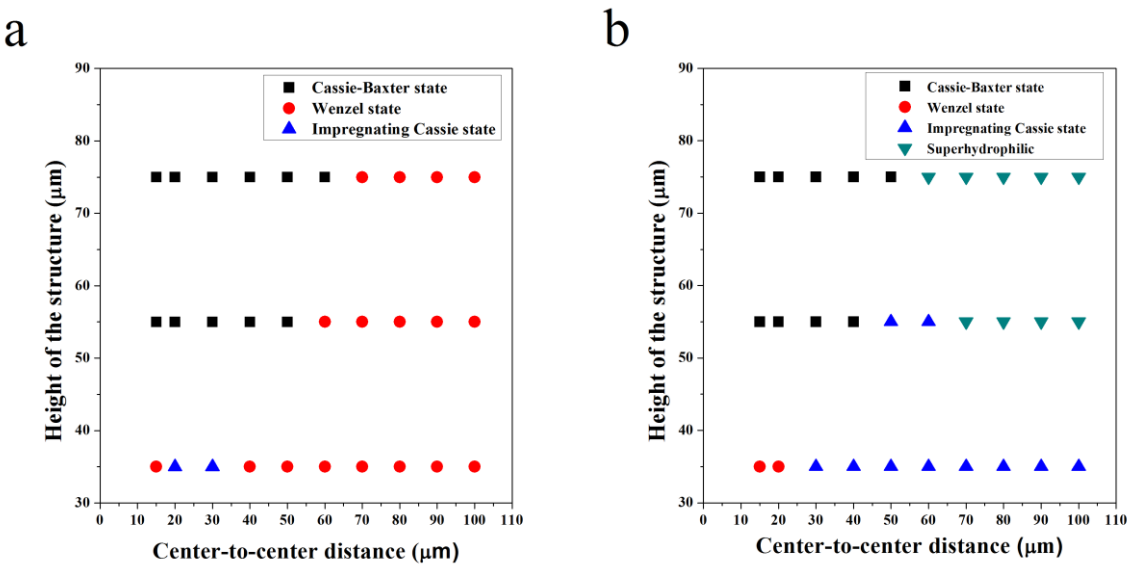

Figure 3. Different wetting states depends on geometrical parameter for (a) truncated cones, (b) hierarchical cones.

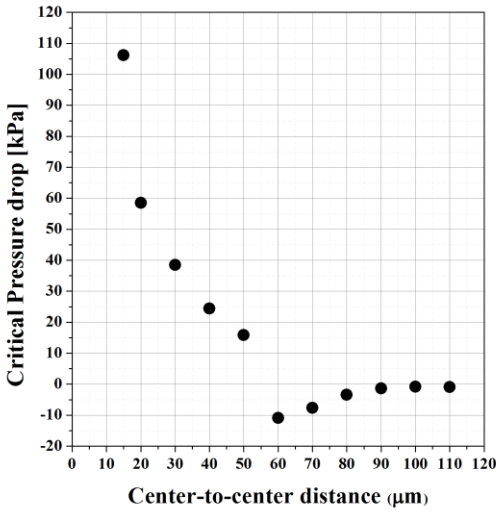

Figure 4. Calculated critical pressure drop for leading to the collapse of the droplet depends on the center-to-center distance based on the parameter from the experiment.

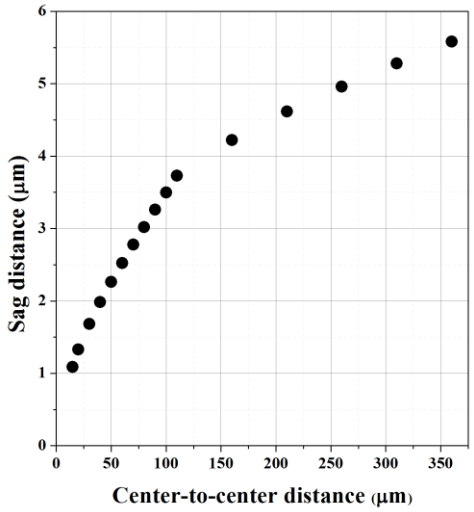

Figure 5. Calculated critical sag distance depends on the center-to-center distance based on the parameter from the fabricated microstructures.

Table 1. RIE etching parameters

	ICP power [Watt]	RF power [Watt]	Temperature [°C]	Pressure [mTorr]	SF_6 flow [sccm]	O_2 flow [sccm]	Time [seconds]
First RIE striking	300	20	-80	20	100	20	10
First RIE etching	500	20	-80	50	100	20	1200, 1800, 2400
Second RIE striking	300	20	-120	20	100	17.5	10
Second RIE etching	500	20	-120	50	100	17.5	1200

Table 2. Parameters of the microstructures

	TC[a] 35	TC 55	TC 75	HC[b] 35	HC 55	HC 75
H_T [µm] [c]	35	55	75	37	58	79
H_P [µm] [d]	4	4	4	4	4	4
H_S [µm] [e]	31	51	71	33	54	75
D_T [µm] [f]	9	9	9	9	9	9
D_B [µm] [g]	30	45	55	30	45	55
P [µm] [h]	15 - 315	15 - 315	15 - 315	15 - 315	15 - 315	15 - 315

[a] Truncated Cone; [b] hierarchical cone; [c] height of truncated cone; [d] height of photoresist; [e] height of silicon; [f] diameter of top surface of truncated cone; [g] diameter of bottom part of conical structure; [h] center-to-center distance.

The wetting transition from Cassie-Baxter state to Wenzel state is shown in this graph.

Two well-fabricated samples which are truncated cone and hierarchical sample show different characteristics on wetting. The sharp Cassie-Wenzel transition is possible to observe in varying center-to-center distance and height, in this study.

Keywords: hierarchical cone, microstructure, wetting transition

Il Woong Park, Maria Fernandino, and Carlos A. Dorao*

Wetting transition of truncated cone and hierarchical cone